Available online at www.sciencedirect.com
ScienceDirect
Journal of Power Sources 179 (2008) 317–328
JOURNAL OF POWER SOURCES
www.elsevier.com/locate/jpowsour

SOFC anodes for direct oxidation of hydrogen and methane fuels containing H_2S

Catherine M. Grgicak, Richard G. Green, Javier B. Giorgi *

Centre for Catalysis Research and Innovation, Department of Chemistry, University of Ottawa, Ottawa, Ontario, Canada K1N-6N5

Received 9 December 2007; accepted 26 December 2007
Available online 4 January 2008

Abstract

Single cell solid oxide fuel cells using Ni-YSZ and Co-YSZ anodes were tested in H_2, CH_4, H_2S/H_2 and H_2S/CH_4 fuel mixtures. Their performance was found to quickly degrade in dry CH_4 due to carbon deposition and lifting of the anode from the electrolyte. In contrast, hydrogen or methane containing H_2S showed an increase in exchange current densities when compared to H_2,M/YSZ/LSM,air systems (M = Ni or Co) despite having less optimal anode microstructure. Conversion from metal to metal-sulfide in the presence of H_2S produced large, dense metal-sulfide particles surrounded by YSZ, thus decreasing the triple-phase boundary. Furthermore, CoS-based anodes showed phase segregation and densification toward the electrolyte. Despite this, long-term testing at $\eta_a = 0.5$ V of the H_2S/CH_4,CoS-YSZ/YSZ/LSM,air system showed no signs of degradation of the anode over a 6-day period. Only after removal of H_2S from the H_2S/CH_4 stream did the CoS-anode reduce back to Co, signifying H_2S is required to maintain the metal-sulfide active anode.

Keywords: SOFC; Anode; Sulfur tolerance; Methane oxidation; Cobalt sulfide; Nickel sulfide

1. Introduction

Solid oxide fuel cells (SOFC) are the most flexible fuel cells with respect to fuel selection. They have great potential for generating power from many sources including hydrogen, natural gas, syngas and biogas. Utilizing natural gas as fuel has procured much attention recently due to its natural abundance, easy transport and accessibility.

Numerous efforts to sustain direct utilization of hydrocarbons in SOFC's have shown that conventional Ni-YSZ (yttria stabilized zirconia) anodes are prone to uncontrolled carbon deposition during operation with dry hydrocarbon feeds since catalytic dissociative adsorption of CH_4 on the anode surface (Eq. (2)) competes with the desired electrochemical reaction (Eq. (1)).

$$CH_4 + 4O^{2-} \rightarrow CO_2 + 2H_2O + 8e^- \quad (1)$$

$$CH_4 \rightarrow C_{gr} + 2H_2 \quad (2)$$

Some researches have attempted to circumvent carbon deposition by using alternative operating conditions, such as adding steam to the fuel stream [1,2]. The anode provides catalytic sites for reforming CH_4 to H_2 and CO. However, internal steam reforming of methane is endothermic and can cause a significant cooling effect with the development of large temperature gradients, while the high H_2O/CH_4 ratio required to avoid coke formation results in a severe decrease of fuel cell open-circuit potential, thereby reducing its efficiency. Additional modifications to operating conditions have focused on introducing oxygen through the electrolyte by increasing the electrochemical load [3].

Other work has focused on preparing alternative anode materials which may be used directly in a dry hydrocarbon environment without changing the operating conditions. To replace Ni-based anodes, alternative materials should be easy to maintain, easy to process and exhibit similar catalytic properties to those of Ni without suffering similar carbon formation. Emphasis has been placed on Cu-based anode materials since they are inexpensive and have been shown to be relatively inert to the formation of C–C bonds. However, the melting temperature of copper and its oxides are low compared to that of Ni and its oxide.

* Corresponding author. Tel.: +1 613 562 5800x6037; fax: +1 613 562 5170.
E-mail address: jgiorgi@uottawa.ca (J.B. Giorgi).

0378-7753/$ – see front matter © 2008 Elsevier B.V. All rights reserved.
doi:10.1016/j.jpowsour.2007.12.082

Therefore, copper anodes cannot be produced as easily as nickel anodes and require pre-sintering of the electrolytic component with pore formers prior to Cu impregnation [4]. Additives such as Mo, Pd, Co, Sm_2O_3 and CeO_2 to Ni- and Cu-based anodes have also been examined and show positive results as they inhibit the formation of adsorbed graphitic layers [5–8]. However, problems associated with cell processing and carbon formation are yet to be resolved.

Natural gas contains fuel impurities; particularly sulfur compounds which also degrade the anodes. Ni-YSZ based systems have shown little tolerance to fuels containing low (ppm) H_2S concentrations, where sulfur tolerance decreased as a function of lower operating temperatures and higher H_2S concentrations [9,10]. However, up to 90% recovery of these systems occurred when H_2S was removed from the fuel, suggesting that poisoning is caused by blocking of the active Ni-YSZ sites by either adsorbed sulfur or H_2S. The small irreversible component was suggested to be the result of NiS formation [10,11]. Studies of nickel–sulfide interactions by Raman spectroscopy at high temperatures suggested NiS is the prevalent species at SOFC operating conditions [12].

Due to the incompatibility of Ni-YSZ based systems with sulfur, emphasis has recently been placed on improving tolerance of SOFC anodes by changing the composition of the anode. Ni-based anodes, where the electrolyte component was changed from yttria-stabilized zirconia (YSZ) to scandia-stabilized zirconia (SSC) showed increased tolerance at 100 ppm H_2S concentrations at 800 °C [9]. Additionally, Cu-ceria anodes exhibited high sulfur tolerance and were able to operate at levels up to 450 ppm at 800 °C without any appreciable loss in performance [13]. An alternative approach was to utilize perovskite structures which can support the oxide-ion vacancies to give good oxide-ion conduction and have a mixed-valent cation from the 4d or 5d block which provides good electronic conduction, while exhibiting high sulfur tolerance. The double perovskites $Sr_2Mg_{1-x}Mn_xMoO_{6-\delta}$ showed long-term stability in 50 ppm H_2S/H_2 at 800 °C, without the formation of sulfur species [14]. Other perovskites also showed potential by exhibiting sulfur tolerance at 1000 °C for up to 8 h in a 1% H_2S/H_2 mixture [15]. Although these materials showed promise in H_2/H_2S fuel mixtures at low concentrations, little evidence on their long-term performance at high sulfur concentrations in methane is available.

This paper represents the first detailed study of Ni-YSZ and Co-YSZ anodes subjected to H_2, CH_4, H_2S/H_2 and H_2S/CH_4 fuel over extended periods of time. The primary objective of this work was to determine the feasibility of employing Ni-YSZ and Co-YSZ cermets as anode materials in multiple fuel environments. Electrochemical measurements were used to determine performance and lifetime of the anodes in each fuel stream. Post-run analysis with SEM, XRD and XPS was used to determine the nature of the active species and any morphological changes.

2. Experimental

The fuel cell was prepared by mixing Triton X-100 (Research Chemical Ltd)/water and 1 g of anode powder. The YSZ supported metal (M-YSZ) (55 wt%) anode materials were prepared via co-precipitation by dissolving appropriate amounts of $ZrCl_4$, Y_2O_3 (dissolved in 10 ml of 37 wt% HCl) and $NiCl_2{\cdot}6H_2O$ or $CoCl_2{\cdot}6H_2O$ (Aldrich) in 165 ml of distilled water. To ensure YSZ phase purity and stability, the anode materials were synthesized with 21 mol% YSZ [16]. Precipitation was achieved through introduction of 2 M NaOH (Aldrich) to pH 13. Following precipitation, the product was filtered, washed, dried at 120 °C and calcined at 750 °C for 2 h. Resulting powder composition and characterization has been described previously [17,18].

0.15 g of the slurry was coated onto an YSZ green-disk (Tosoh) and heated to 1400 °C for 4 h in air. A 70 wt% LSM/30 wt%YSZ mixture (LSM, Nextech Materials; YSZ, Tosoh) was used as the cathode and reference electrode material. The cathode was prepared by coating 0.15 g of LSM/YSZ powder symmetrically opposing the sintered anode, while the reference electrode was approximately 4 mm to the side of the cathode [19]. Upon sintering, the YSZ electrolyte was 0.5 mm thick with electrode areas of 0.4 cm^2 for the anode and cathode and 0.2 cm^2 for the reference electrode. Both numerical and experimental findings suggest that ideal SOFC three-electrode geometry would include a symmetric cell where the counter and working electrodes are symmetrically opposed to one another with the reference electrode as far away from them as possible [20,21]. Also, by increasing the electrolyte thickness, errors associated with electrode misalignment would be minimized. However, a compromise regarding electrolyte thickness is needed given that it must be thin enough to allow reasonable current densities and thick enough to keep electrode alignment errors minimal [19]. A full depiction of the cell setup has previously been described [22].

The choice of current collector and its incorporation into a SOFC is important to develop systems with high power output and/or to study the electrochemical behavior of an electrode material. The current collector should not participate chemically or electrochemically in the electrode reaction and the overall cell resistance should not be significantly affected by any current constriction caused by inadequate contact between electrode and current collector. In this light, two main types of current collectors are used: paste and mesh. Paste can easily be coated onto the electrode and the contact area between current collector and electrode can be determined with accuracy. However, paste current collectors have been shown to modify the physical structure of the electrode over time by decreasing the number of reaction sites [24]. In contrast, mesh current collectors are reusable but significantly affect polarization losses, where current constriction decreased with increased mesh contacts [23].

To address the aforementioned concerns, the current collector used in these systems was a Pt-10%Rh mesh with a 0.003 in. wire diameter (Unique Wire Weaving Co.) embedded into the electrodes. Embedding the mesh relieves the concerns associated with contact resistance however it is difficult to ensure flat electrode surfaces across the area. However, since the active thickness of fine Ni-YSZ cermet anodes have been demonstrated to be in the range of 10 μm [25], while the rest of the anode acts as a current carrier, the regularity of the surface was

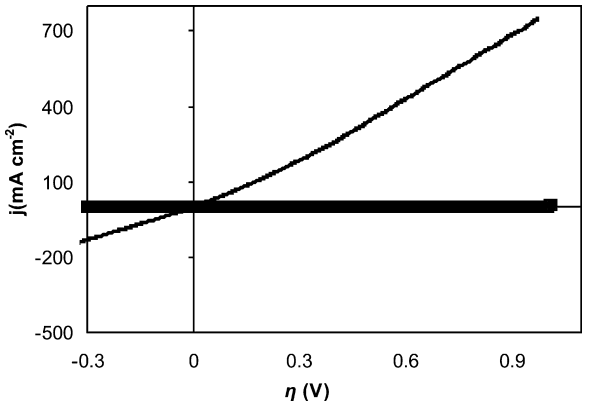

Fig. 1. Current density versus overpotential (without *iR* compensation) curves for (–) Ni-YSZ electrode and (■) YSZ electrode with embedded Pt-10%Rh current collector.

not taken into consideration (the active electrode cross-sections were consistently much larger than 20 μm).

Issues related to the electrochemical activation by the mesh were addressed prior to fuel cell testing. Fig. 1 shows the current density versus overpotential results for a commercially purchased Ni-YSZ anode (Fuel Cell Materials) and an YSZ 'blank' anode. Both measurements were performed using the embedded Pt-10%Rh mesh as the current collector. Large differences in current densities are observed for each fuel cell. The anode consisting of YSZ and Pt-10%Rh mesh exhibited a maximum current density of ~4 mA cm^{-2}, while the anode utilizing commercial Ni-YSZ exhibited current densities as high as 750 mA cm^{-2}. The low current densities observed in the 'blank' anode show the current contributions from the embedded mesh are minimal and therefore were not taken into consideration during electrochemical analysis. This is attributed to the small TPB area between mesh, gas and YSZ.

Hydrogen, methane and hydrogen sulfide flows were regulated by mass flow controllers (MKS) to a total flow of 50 sccm. Temperature was controlled via an Omron E5CN controller and measured with a K-type thermocouple placed outside a shielded quartz tube. The Chromel®-shielded quartz tube was placed in the furnace around the fuel cell, connected to ground and used as a precaution to reduce background noise introduced by the furnace.

Electrochemical measurements were performed at 850 °C with the following fuels: pure hydrogen, pure methane, 10% (v/v) H_2S/H_2 or 0.3–10% (v/v) H_2S/CH_4. Pyrex® was used to seal the edge of the alumina tube to the YSZ surface. After initial preparation, mounting and reduction of the cell, a minimum OCV of 1.0 V in H_2 was required to continue electrochemical measurements. All such measurements were taken using a VoltaLab 40 (Radiometer Analytical), where impedance measurements were taken over a frequency range of 100 kHz–250 mHz at OCV. Equivalent circuit modeling of impedance data was performed with Zview software. DC current-voltage measurements were conducted using a potential scan rate of 2 mV s^{-1}. Exhaust gas was monitored using an AccuQuad residual gas analyzer. Pre- and post-run analysis of the fuel cell anode was accomplished by X-ray diffraction (XRD) (Phillips PW1830) using CuKα radiation with a wavelength of 1.54 Å. The scan range was measured from $2\Theta = 20^\circ$ to 90° at a rate of 0.02° s^{-1}. Crystalline phases were assigned using the Powder Diffraction File (PDF) database (ICCD, 2001, Dataset 1-51). NanoLab7 SEM with Kevex EDS was used to assess particle size and morphology as well as elemental compositions.

X-ray photoelectron spectroscopy (XPS) experiments were performed in a SPECS Gmbh. multi-technique ultra-high vacuum chamber with a base pressure of 10^{-10} mbar. A non-monochromated source producing aluminum Kα X-rays (1486.7 eV) was used and survey spectra in the binding energy range 1200-1 eV were taken (0.8 s dwell, 0.3 eV step). The electron pass energy was set to 10 eV. Higher resolution scans of selected peaks were performed for quantification and comparison purposes (8 s dwell, 0.2 eV step), and were fit in Casa XPS analysis software using a mixed Gaussian-Lorentzian function after Shirley background subtraction. The Binding energy scale was calibrated to the carbon peak which was set to 284.8 eV. Atomic percent concentrations were determined from representative peak areas after dividing by their relative sensitivity factor given in the Scofield library.

3. Results and discussion

3.1. Performance of Ni-YSZ and Co-YSZ anodes in CH_4

Prior to fuel cell operation, SEM images of anode/YSZ electrolyte cross-sections were taken and are exhibited in Fig. 2. The NiO-YSZ anode in Fig. 2a shows porous microstructure and good contact between anode and electrolyte. The Co_3O_4-YSZ anode in Fig. 2b shows a very different morphology and is characterized by large YSZ particles surrounded by Co_3O_4. Contact between the Co_3O_4-YSZ and electrolyte is also satisfactory.

The progression of current versus overpotential (iR_s corrected) behavior is shown in Fig. 3a and b for Ni-YSZ and Co-YSZ anodes with time after CH_4 addition. The first measurement was taken with hydrogen as fuel. Due to the slow scan rate, a current reading was taken approximately every 1–1.5 mV. For purposes of clarity, these figures show the currents obtained every 25 mV.

Fig. 4 is a summary of these results and shows the ratio of exchange current densities obtained with CH_4 and H_2 fuels for Ni- and Co-YSZ anodes. Ratio of exchange current densities between the fuel of interest and H_2 were used to account for deviations associated with irreproducibility between fuel cells and therefore represent a direct measure of the change in performance over time for each cell.

Exchange current densities were obtained using the generalized kinetic equation for a one-electron transfer process proposed by Erdey-Gruz and Volmer and Butler [26–29].

$$i = i_o \left\{ \exp\left[\frac{\alpha_a \eta F}{RT}\right] - \exp\left[-\frac{\alpha_c \eta F}{RT}\right] \right\} \quad (3)$$

where i is the current density, i_o the exchange current density, α is the transfer coefficient, η the overvoltage and F, R, T are the Faraday constant, ideal gas constant and temperature, respectively.

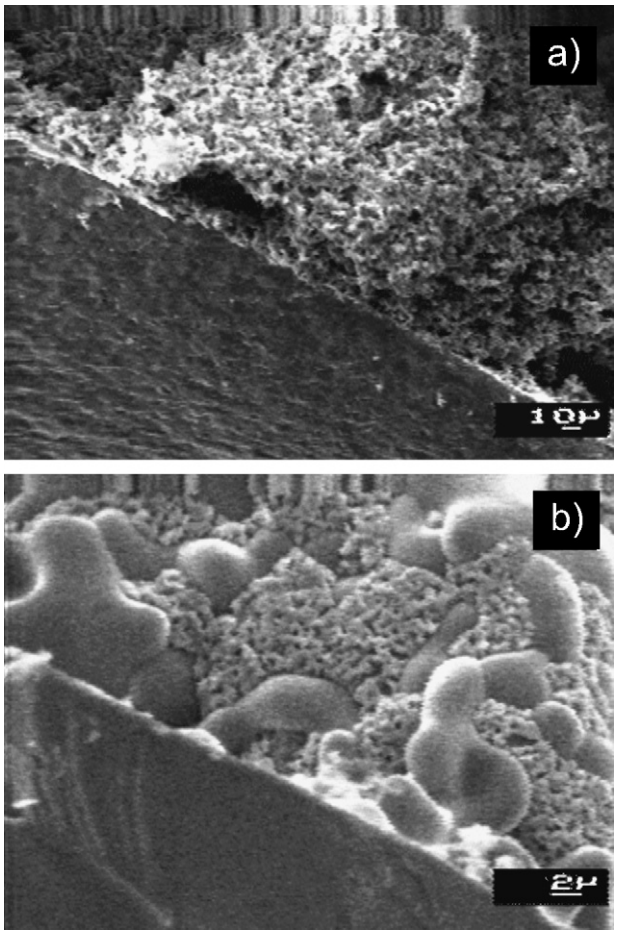

Fig. 2. Cross-sections of YSZ and anode powders after sintering on dense YSZ. (a) NiO-YSZ; (b) Co_3O_4-YSZ.

This relation takes into account both the forward and reverse reactions for the process and the exponential potential dependence of the current components through the transfer coefficients α_a and α_c.

For appreciable positive polarizations the second term of Eq. (3) becomes negligible and the expression simplifies to

$$\ln i = \ln i_o + b^{-1}\eta \quad \text{where } b^{-1} = \frac{\alpha_a F}{RT} \tag{4}$$

By plotting $\ln i$ versus η, one may obtain both the exchange current density for a particular reaction and the inverse Tafel slope. Fig. 3c and d show the relationship between ln(current), iR_s-corrected overpotential and the subsequent Tafel behavior for the Ni-YSZ and Co-YSZ samples run in H_2 and CH_4 (after $t = 15$ h), y. The quantity of R_s was obtained as the high-frequency intercept of the impedance spectrum for each respective temperature. The overpotential range was not restricted since there was no indication of passivation. The Tafel region was calculated between 400 and 550 mV, but spanned a much larger overpotential region (~1 decade). Since the Butler-Volmer equation assumes that the electrochemical activation is directly related to changes in the electrochemical free energy of the system, concerns regarding mass diffusion or adsorption effects were considered. Previous work in this laboratory indicated the electrochemical responses were due to charge transfer reactions and not adsorption or diffusion processes. More specifically, impedance spectroscopy showed the third low frequency response, which is usually attributed to 'gas conversion', was not observed at $\eta > 200$ mV, suggesting simple gas diffusion limitations based on Fick's Law should not be used to describe this element. Furthermore, activation energies (90+/−10 kJ mol^{-1} for Ni-YSZ and 130+/−10 kJ mol^{-1} for Co-YSZ) calculated using this technique also suggested the electrochemical responses were due to charge transfer reactions [22].

Upon operation with dry methane, the Ni-YSZ anode exhibited a slight increase in performance in the first 5 h, but quickly began to degrade after 5 h of operation (Fig. 4). By the 15th hour, the anode had fully degraded and showed no activity. Post-run analysis showed the anode had disintegrated and black powder found at the bottom of the fuel cell was collected for analysis. Unlike Ni-YSZ, Co-YSZ exhibited an $i_oCH_4/i_oH_2 < 1$ at all times with no noticeable signs of decreasing performance during 15 h of testing. However, post run analysis of this anode showed that the edges of the Co-YSZ anode had begun to separate from the electrolyte leading us to believe that this anode would also lose performance upon further use.

XRD analysis of the black powder found at the bottom of the Ni-YSZ fuel cell consisted of Ni (PDF# 04-0850), YSZ (PDF# 30-1468) and graphite (PDF# 26-1077). Post-run XRD of the Co-YSZ anode itself showed the presence of hexagonal Co (PDF# 05-0727), YSZ and small amounts of graphite.

Low resolution SEM/EDX of post-run anodes in Fig. 5 revealed the morphology of the anodes after 15 h in dry methane. It was clear that the Ni-YSZ anode had degraded producing the powder containing a significant amount of graphite with no visible signs of the original Ni or YSZ sintered bodies. Co-YSZ anodes resulted in a portion of the anode disengaged from the electrolyte and another portion still attached to it. Fig. 5b shows a section of the anode which was separated from the electrolyte. The large crystalline particles approximately 2–6 μm in diameter were YSZ, while the smaller particles consisted of Co and possibly graphite as shown by EDX analysis. Fig. 5c is the portion of the anode which did not disengage from the electrolyte and shows the sintered YSZ and Co morphology as seen prior to fuel cell operation in methane, albeit with separation between the Co and YSZ bodies.

The tendency of metals to form carbon has been well studied particularly for catalytic applications [30–33]. Carbon formation involves deposition of a carbon source onto the metal surface, its dissolution into the bulk, and its precipitation back out as a fiber at the surface of the metal particle. Therefore the metal phase can be physically lifted from the electrolyte by carbon. This lifting is noticeable in the Co-based anode where the Co species in Fig. 5c are clearly separated from YSZ. This would eventually lead to the disintegration of the anode from the YSZ component. Although the Co-based anode showed no electrochemical decrease in performance during 15 h of operation, SEM and XRD analysis suggested this fuel cell would eventually suffer full degeneration once enough graphite was produced to fully separate the components from each other.

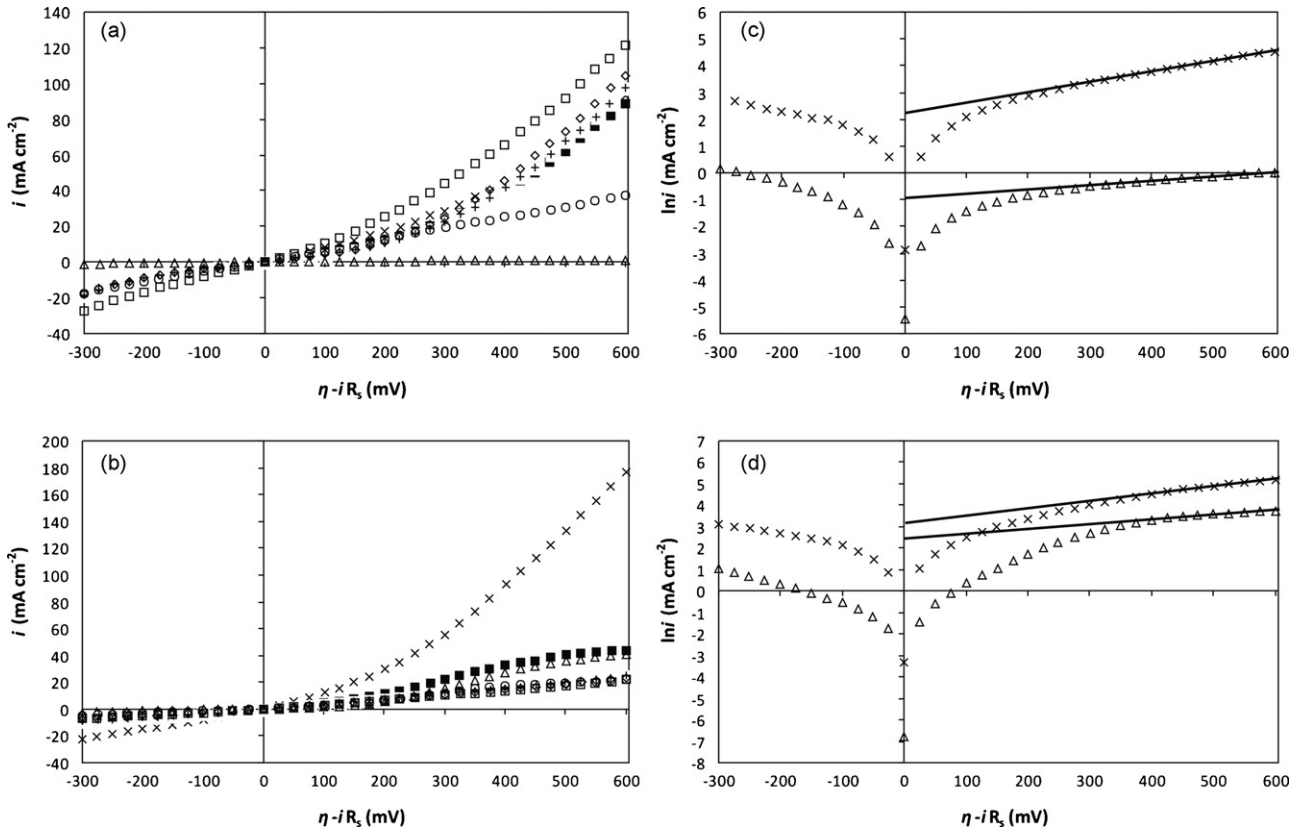

Fig. 3. Current–overpotential relations for the anodic and cathodic portions of the η versus i curves at 850 °C in CH_4 for (a) Ni-YSZ and (b) Co-YSZ anodes at (×) $t = 0$ (pure H_2), (■) $t = 1$ min, (+) $t = 1.5$ h, (◊) $t = 3$ h, (□) $t = 5$ h, (◯) $t = 10$ h and (△) $t = 15$ h. (c) and (d) are examples of the ln(current)–potential relations and Tafel behavior for Ni-YSZ and Co-YSZ anodes at $t = 0$ (pure H_2) and $t = 15$ h, respectively.

3.2. Performance of Ni-YSZ and Co-YSZ anodes in H_2S containing fuels

3.2.1. H_2S/H_2

Fig. 6a and b show the progression of current versus overpotential (iR_s corrected) behavior for Ni-YSZ and Co-YSZ anodes with time after 10% (v/v) H_2S addition. Fig. 6c and d are the ln(current) and overpotential relations. The first measurement was taken with hydrogen as fuel.

Qualitatively, it was observed that near OCV, small anodic peaks were occasionally observed in H_2S/H_2 atmospheres that were not present when H_2 was the fuel. This is particularly obvious for Ni-YSZ samples at times 0, 1 min, 1.5 h, 3 h, 5 h and 10 h (Fig. 6a). Previous cyclic voltammetry experiments on similar samples performed in this laboratory show that the process was irreversible in H_2S atmospheres [22]. CV studies at various operating conditions are required to fully determine the nature of these peaks, however, previous studies on Cu_2S by Nava et al. suggest that they may be related to serial oxidation of the metal-sulfides through defective sulfides [34].

Fig. 7 shows the change in the ratio of exchange current densities for Ni-YSZ and Co-YSZ anodes with time when H_2S is added to H_2. The results indicated Ni-YSZ and Co-YSZ cermet anodes were initially ($t = 1$ min) degraded by the sulfide impurity with $i_oH_2S/H_2/i_oH_2 < 1$. However, by $t = 1.5$ h the performances noticeably increased. After $t = 3$ h the resistances remained relatively constant. The Co-based anode reached peak performance at $t = 3$ h, but showed signs of degradation past this point. The Ni-based anode did not exhibit a significant improvement in performance with H_2S however it did not seem to degrade over this time scale.

XRD analysis of post run anodes indicated the addition of high levels of H_2S into the fuel stream produced anodes consisting of NiS- and CoS-species. More specifically, the Ni-YSZ anode consisted of Ni_3S_2 (PDF# 44-1418) with traces of $NiS_{1.03}$(PDF# 02-1273), while the Co-YSZ anode was Co_3S_4(PDF# 44-1738) and Co_9S_8(PDF# 02-1459). The phases present at room temperature are not assumed to be the electrode present during fuel cell operation at high temperatures. The existence of metal-sulfide species at low temperature demonstrated

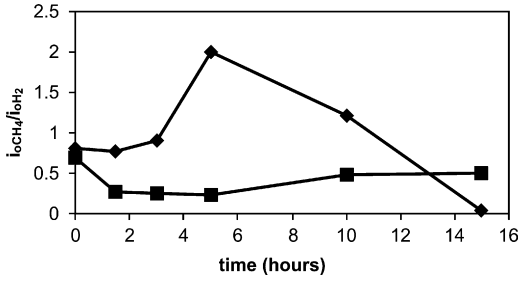

Fig. 4. Changes in exchange current densities of Ni-YSZ and Co-YSZ anodes over time in CH_4. (♦) Ni-YSZ (■) Co-YSZ.

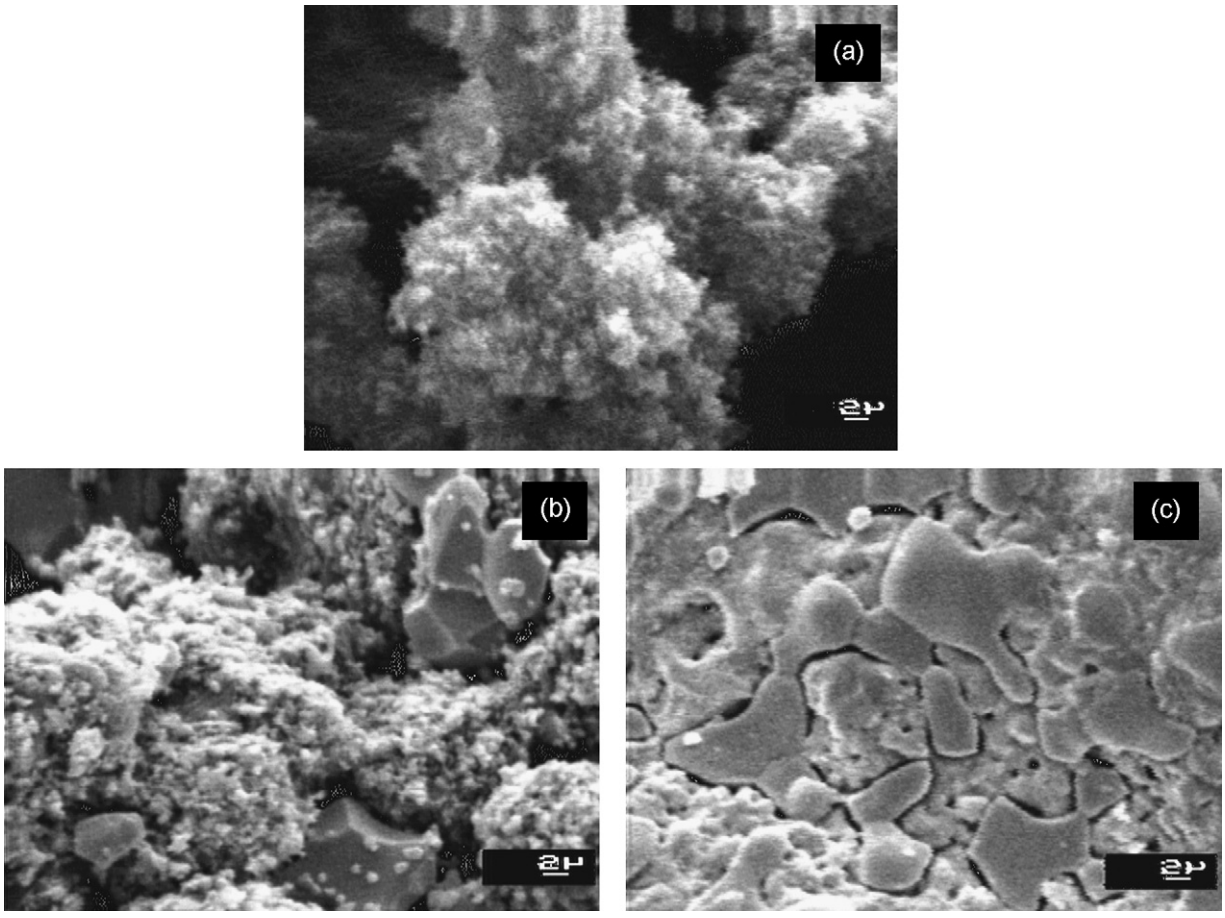

Fig. 5. SEM images of top views of the anodes microstructure after operating at 850 °C for 15 h in CH_4. (a) Ni-YSZ; (b) Co-YSZ and (c) Co-YSZ in contact with the electrolyte.

that metals were converted to metal sulfides during operation with H_2S. In situ analysis would be required to conclusively determine the exact species of MS- present during operation. However, sulfidation studies of cobalt and nickel suggest the active species at fuel cell operating temperatures are $Co_{1-x}S$ and $Ni_{3+x}S_2 + Ni_{1-x}S$, respectively [35,36]. Since the exact metal sulfide species at high temperatures is not known, the sulfide anodes will be referred to as NiS- and CoS-YSZ.

The increase in polarization of the anode during the first minutes of H_2S introduction is consistent with results obtained with low H_2S concentrations [9–11] and may be the result of initial blocking of reactive sites by sulfur species or by agglomeration of metal particles accelerated by the presence of sulfur. With increased exposure time, all the metal is converted to metal-sulfide and a decrease in polarization occurred, suggesting deactivation at low concentrations over short periods of time was the result of transition states between metal and metal-sulfide phases. Once all the metal is converted, the active metal-sulfide catalyst may be used as a viable anode material for H_2S containing fuels. The reversible transition between metal and metal-sulfide phases is possible. Therefore, to maintain structural and compositional purity of metal-sulfide anodes, H_2S would continuously be required in the fuel stream.

The ability to electrochemically oxidize H_2S in a fuel cell has previously been established. This was first demonstrated by Pujare et al. by utilizing thiospinel $CuFe_2S_4$ as the anodes' electrocatalytic site and pure H_2S as fuel [37]. Additionally, anode catalysts comprising of composite metal sulfides derived from a mixture of sulfides of Mo and other transition metals (Fe, Co, Ni) were stable and effective electrocatalysts for conversion of H_2S in SOFC's, with Co-Mo-S exhibiting superior activity and longevity [38,39]. Although these data suggested metal-sulfides are viable SOFC anodes for H_2S containing fuels, very little is understood regarding the H_2S oxidation reaction, which was emphasized by larger than expected OCV values obtained in these cases.

When utilizing H_2S as fuel with an oxide-conducting electrolyte the reaction that takes place at the cathode is the same as in the conventional case when hydrogen is used and is represented by the following equation

$$\tfrac{1}{2}O_2 + 2e^- \rightarrow O^{2-} \tag{5}$$

After migration through the electrolyte the oxide ions can react with hydrogen sulfide at the anode yielding two possible overall reactions:

$$H_2S + O^{2-} \rightarrow H_2O + \tfrac{1}{2}S_2 + 2e^- \tag{6}$$

$$H_2S + 3O^{2-} \rightarrow H_2O + SO_2 + 6e^- \tag{7}$$

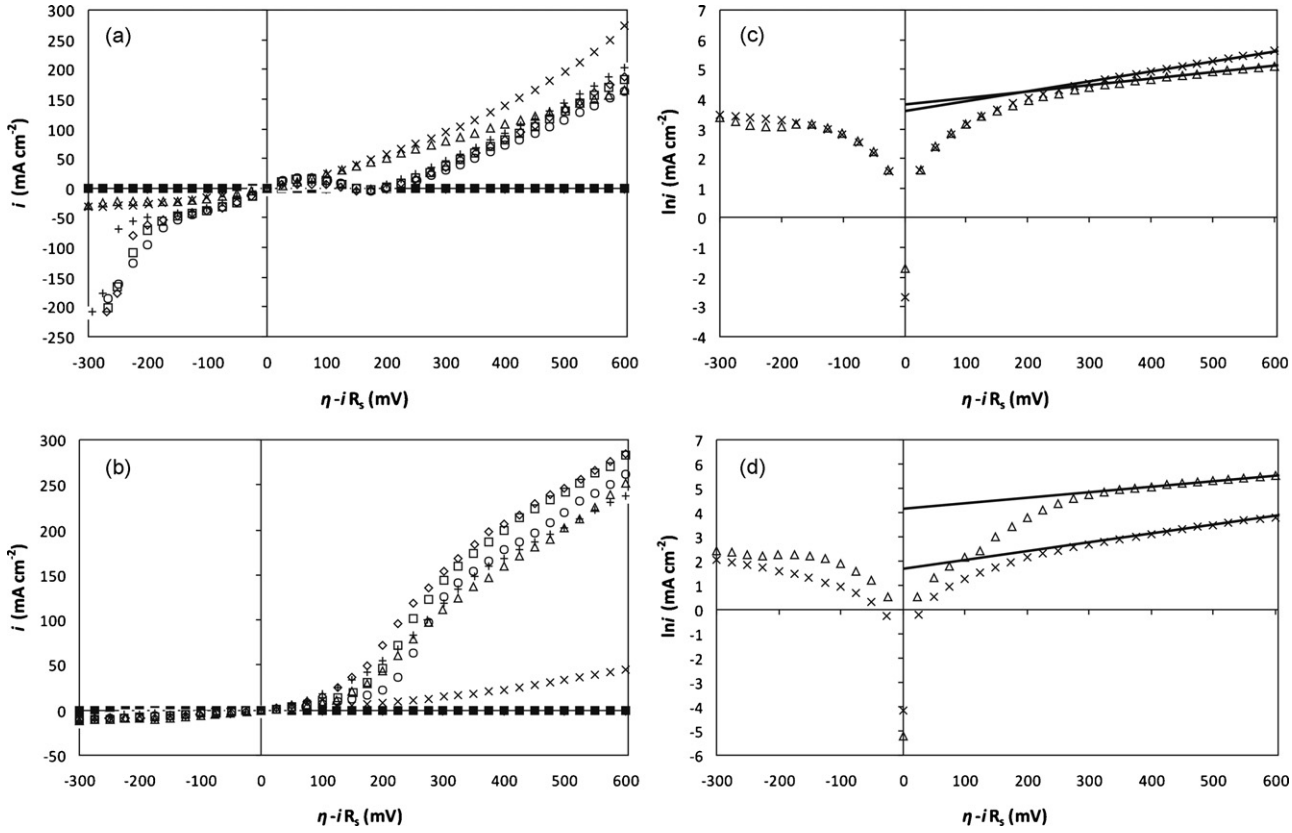

Fig. 6. Current–overpotential relations for the anodic and cathodic portions of the η verses i curves at 850 °C in 10% (v/v) H_2S/H_2 for (a) Ni-YSZ and (b) Co-YSZ anodes at (×) $t = 0$ (pure H_2), (■) $t = 1$ min, (+) $t = 1.5$ h, (◊) $t = 3$ h, (□) $t = 5$ h, (◯) $t = 10$ h and (△) $t = 15$ h. (c) and (d) are examples of the ln(current)–potential relations and the Tafel behavior for Ni-YSZ and Co-YSZ anodes respectively at $t = 0$ (pure H_2) and $t = 15$ h.

where the reversible potentials are 0.726 V and 0.750 V at 800 °C, respectively. The process may further be complicated by thermal decomposition of hydrogen sulfide at the anode via

$$H_2S \rightarrow H_2 + \tfrac{1}{2}S_2 \tag{8}$$

thereby introducing hydrogen which may also be oxidized. Therefore higher than expected OCV values (∼1 V) observed in these systems may be explained by the reaction of H_2.

Moreover, the products of Eqs. (6) and (8) may be further oxidized

$$\tfrac{1}{2}S_2 + 2O^{2-} \rightarrow SO_2 + 4e^- \tag{9}$$

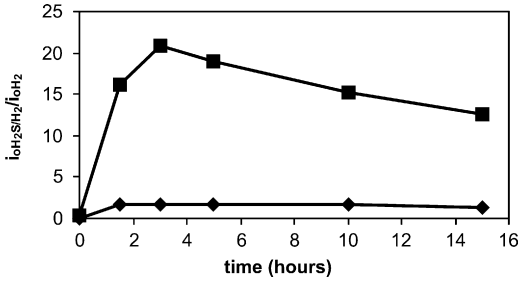

Fig. 7. Changes in exchange current densities of Ni-YSZ and Co-YSZ anodes over time in 10% (v/v) H_2S/H_2. (♦) Ni-YSZ (■) Co-YSZ.

Reactions between excess H_2S and SO_2 may also take place via the second step of the Claus process

$$2\,H_2S + SO_2 \rightarrow 2H_2O + 3/nS_n \qquad n = 2\text{–}8 \tag{10}$$

where n is the average molecular species of the sulfur product. However, since reaction (10) is an equilibrium reaction favored at low temperatures and high SO_2 partial pressures, significant H_2O and S_n production is not expected at high H_2S concentrations and SOFC operating temperatures.

By studying the product distribution of the H_2S, $Pt|(Ce_2)_{0.8})(SmO_{1.5})|Pt$, air system, Peterson et al. suggested complete oxidation of hydrogen sulfide to sulfur dioxide was the preferred product [40]. However, it was impossible to determine whether the reaction took place via a two step (via Eq. (6) and (9)) or one step process (via Eq. (7)) since both require a $6e^-$ transfer. In our results, analysis of exhaust gas by mass spectrometry indicated that there was not a significant amount of SO_2 production, which would otherwise be expected if the main fuel was H_2S and not H_2. Additionally, there was no evidence of solid sulfur formation once the fuel cell was examined after a 15 h period. The main increase in performance over time was assumed to be the ability of metal-sulfide electrodes to oxidize hydrogen at an appreciable and continuous rate. This is in agreement with OCV values obtained when H_2S/H_2 was used as fuel. The OCV's of Ni-YSZ and Co-YSZ anodes in H_2S/H_2 at 850 °C were 1.1 V and 1.2 V, respectively. The slight discrep-

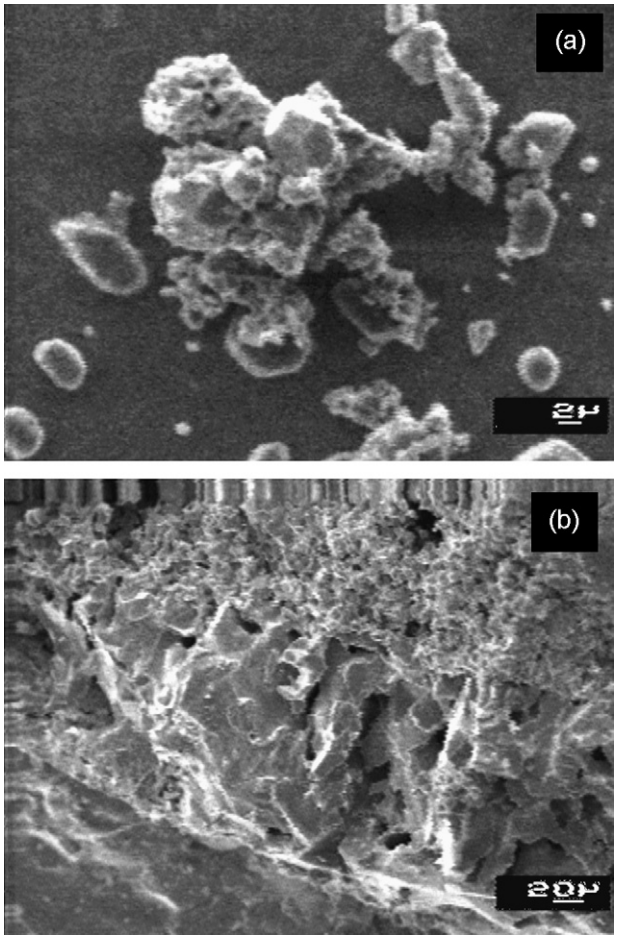

Fig. 8. SEM images of anodes' microstructure after operating at 850 °C for 15 h in 10% (v/v) H_2S/H_2. (a) Section of Ni-YSZ anode (b) Cross-section of Co-YSZ on dense YSZ electrolyte showing phase segregation of newly formed CoS- toward the electrolyte.

ancy between the OCV values of each anode was attributed to irreproducibility of the seal between fuel cells. These values are similar to the OCV's of 1.2 obtained when H_2 was used as the fuel. OCV's for both Ni-YSZ and Co-YSZ in H_2S/H_2 are very different from those calculated from thermodynamic data for oxidation of H_2S which is approximately 0.75 V at 850 °C. Although small contributions from oxidation of H_2S cannot fully be excluded, it is suggested that oxidation of hydrogen on metal-sulfides was the main electrochemical reaction.

Fig. 8 shows the SEM/EDX analysis of post-run anodes tested in 10% (v/v) H_2S/H_2. Fig. 8a shows a portion of the Ni-based anode which was removed from the electrolyte. Large crystal species ranging in size from 2 to 100 μm (100 μm not shown) in diameter were present throughout the anode. EDX shows the large crystalline particles were NiS- while the less compact section was a combination of NiS- and YSZ. The SEM cross-sections of the Co-based anodes in Fig. 8b show phase segregation toward the electrolyte not observed prior to fuel cell operation. A dense layer consisting of CoS- was next to the dense YSZ, while the porous structure on the top consisted of CoS- and YSZ. This segregation of dense, non-porous CoS- toward the electrolyte would significantly decrease the triple

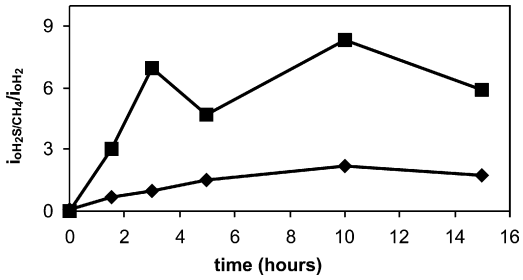

Fig. 9. Changes in exchange current densities of Ni-YSZ and Co-YSZ anodes over time in 10% (v/v) H_2S/CH_4. (♦) Ni-YSZ (■) Co-YSZ.

phase boundary between metal, YSZ and gas, and would explain the decrease in performance of the Co-based anode in H_2S/H_2 over time. Therefore, changes in morphology during CoS- formation cause the decrease in exchange current densities over time. Since these anodes were made in situ by addition of H_2S to the fuel stream, optimizing the NiS- or CoS-YSZ microstructure was not performed. Developing methods which allow for fabrication and optimization of metal sulfide anodes are necessary to fully elucidate the potential of these metal-sulfide anodes. Improvement of NiS- and CoS-microstructure should result in fuel cell anodes with higher and more stable current densities than those of the well known Ni-based anodes.

3.2.2. H_2S/CH_4

When H_2S/CH_4 was used as fuel, a decrease in performance was initially observed. However, as with the H_2S/H_2 system, the performance quickly increased and exceeded that observed when H_2 was the fuel. The improvement is evidenced by the large $i_oH_2S/CH_4/i_oH_2$ ratios (Fig. 9).

Formation of NiS- and CoS-species was again deemed to be the cause of the initial decrease in performance. Once all the metal converted to metal-sulfide, a marked increase in performance was again observed. Both the NiS- and CoS-systems showed remarkable improvement in the presence of methane and H_2S, producing exchange current densities which were ∼1.5 and ∼6 times greater, respectively than those obtained when dry hydrogen was the fuel. Neither fuel cell showed signs of degradation over a 15 h period.

XRD analysis of post run anodes indicated addition of high levels of H_2S into the fuel stream resulted in anodes consisting of NiS- and CoS-species. More specifically, the Ni-YSZ anode consisted of Ni_7S_6 (PDF# 14-0364), $NiS_{1.03}$(PDF# 02-1273) and Ni_xS_6 (PDF# 51-0718), while the Co-YSZ anode was $CoS_{1.035}$(PDF# 25-1081). Again, the phases present at room temperature are not assumed to be the electrode present during fuel cell operation at high temperatures and are possibly $Co_{1-x}S$ and $Ni_{3+x}S_2 + Ni_{1-x}S$ as suggested previously [35,36].

Post-run analysis of the fuel cell showed that unlike the H_2S/H_2 system, a silvery foil like substance was found near the anodes and along the edges of the tube. XRD of this substance showed that it was amorphous and characterization via powder X-ray diffraction was not attempted. SEM analysis of this substance was performed as shown in Fig. 10.

The foil consisted of flat plate like particles approximately 10 μm in diameter. Two foil samples were studied by X-ray pho-

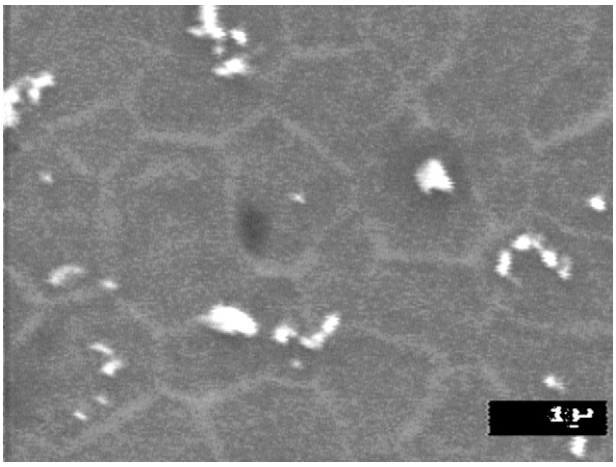

Fig. 10. SEM image of the foil produced during H_2S/CH_4 Co-YSZ fuel cell operation.

toelectron spectroscopy, in the first sample the surface of the foil in contact with the alumina tube was analyzed (Fig. 11a), in the second the outside surface was considered. In the first sample, the foil surface region was composed of carbon, oxygen, sulfur, and sodium in relative atomic concentrations of 66%, 24%, 6%, 4%, respectively. The sodium was not seen in the second sample and was likely released from the Pyrex ring during its melting for initial seal formation. The sulfur 2p peak (Fig. 11b) however, was seen in both samples, and it was found to be split, with one peak at a binding energy of 164 eV and the other at 169.8 eV.

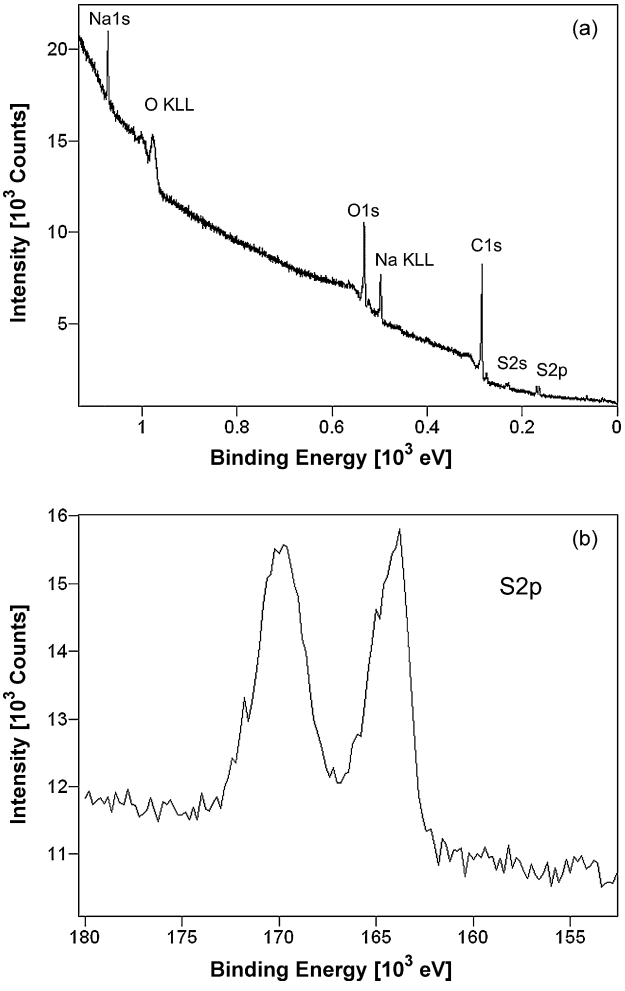

Fig. 11. (a) XP-survey spectrum (1100-0 eV) of the amorphous carbon sample surface which was in contact with the alumina tube. (b) High resolution scan of the split sulfur 2p peaks.

The former likely corresponded to elemental sulfur (164 eV) or a chemisorbed sulfide such as CS_2 (163.7 eV) [41], and the latter derived from an oxygen containing sulfur species such as a sulfone (∼167–170 eV) or sulfate (∼168–171 eV) [42]. The amorphous carbon foil itself likely grows in a manner similar to a chemical vapor deposition (CVD) type mechanism, in which precursor gases react or decompose at a substrate surface forming a film. These types of films are often grown by various types of CVD such as plasma enhanced CVD or hot filament CVD in which the precursors are altered in order increase growth rate. However these added techniques are not necessarily required and the high temperatures of the fuel cell may produce the same results. There is a large body of literature in which carbon films are formed by CVD using methane and hydrogen as precursor gases [43–45]. Typically temperature and precursor ratios control the film structure from amorphous to crystalline. XP-spectra of sulfur doped micro and nano-crystalline carbon films grown by Gupta et al. [45] using CH_4, H_2 and H_2S as precursors showed a split sulfur 2p peak similar to the one observed in the foil. By depth profiling it was found that the elemental sulfur was incorporated throughout the film while the oxygen containing sulfates or sulfones were absorbed only on the surface. Furthermore these films grew at an increasing rate with H_2S concentration. In fact it was shown that the growth rate at 900 °C increased from around 0.1 $\mu m\,h^{-1}$ at 0–200 ppm to about 4.3 $\mu m\,h^{-1}$ at 500 ppm. One explanation proposed by the authors for this increase was that the introduction of sulfur to the system, which absorbed to the substrate surface, provided nucleation points for carbon, increasing the rate of film growth. However the mechanism proceeded, it is clear the introduction of H_2S affects the reaction mechanism for gases in the fuel cell accelerating the growth of the carbon film. This explains why the foil was formed in the fuel cell using CH_4/H_2S, and not using CH_4 alone.

Analysis of exhaust gas by mass spectrometry indicated there was not a significant amount of SO_2 produced, yet there was CS_2 production according to the following reaction

$$CH_4 + 2H_2S \rightarrow CS_2 + 4H_2 \quad (11)$$

Other possible products such as CH_3SH and C_2H_5SH were not observed in the mass spectrum [46].

OCV values obtained for these systems were 1.0 V and 1.2 V for the Ni-based and Co-based anodes, respectively. The introduction of CS_2 as an electrochemically active species renders determination of the fuel impossible since CS_2 may be oxidized in numerous ways. Despite, mass spectrum data showing no significant signs of COS or SO_2 production, the possibility of the measured OCV resulting from electrochemical oxidation of a combination of H_2, CH_4 or CS_2 is not excluded.

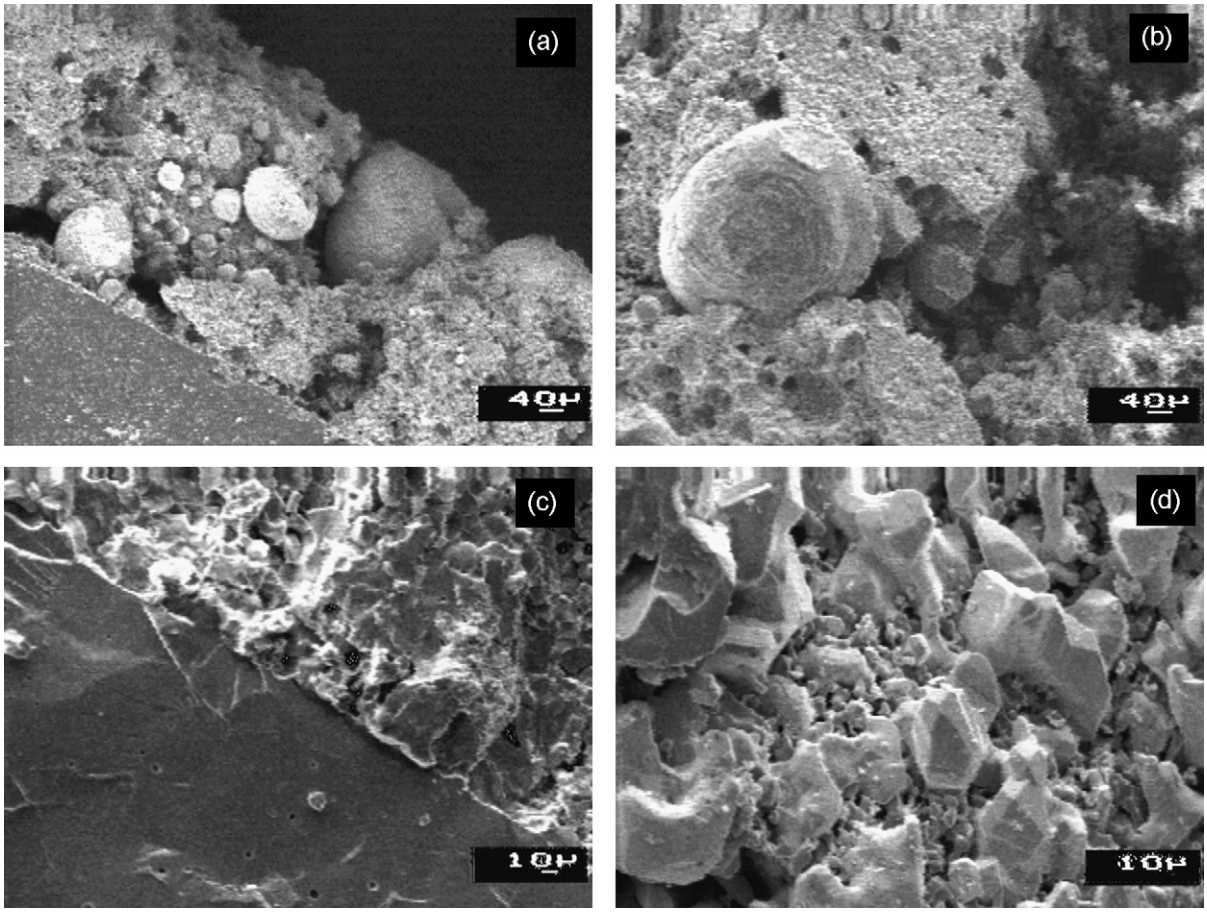

Fig. 12. SEM images of Ni-YSZ and Co-YSZ anodes after operating at 850 °C for 15 h in H_2S/CH_4. (a) Cross-section of Ni-YSZ on dense YSZ; (b) top view of Ni-YSZ anode; (c) cross-section of Co-YSZ on dense YSZ; (d) top view of Co-YSZ anode.

SEM/EDX post-run analysis of the anodes shows relatively good contact for both the Ni-based and Co-based anodes (Fig. 12a and c). The Co-YSZ anode showed a very dense structure near the electrolyte consisting of CoS- and YSZ. Fig. 12d is the top view of the anode and shows large particles consisting of a CoS- phase surrounded by smaller YSZ particles. The large increase in activity of these systems with respect to H_2 demonstrates the exciting prospect of using metal-sulfides as anodes for oxidation of sulfur containing natural gas, despite the high density of the CoS-YSZ anode and consequent reduction of the TPB. Similar results are observed for NiS-YSZ anodes where large particles of NiS-species dominated the anode microstructure (Fig. 12a and b).

To assess the feasibility of using CoS-YSZ as a potential fuel cell anode, the cell was left to run for a total of 6 days at 850 °C in 10% (v/v) H_2S/CH_4. Fig. 13 shows the H_2S/CH_4,CoS-YSZ/YSZ/LSM,air system run continuously at an anodic overpotential of 500 mV ($\eta_a = 500$ mV) without any noticeable degradation. The reason for consistent increase in current densities over time is yet unclear. Studies which regulate the morphology of CoS-YSZ anodes would be required to assess the feasibility of utilizing these materials in fuel cell stacks.

When H_2S was removed from the system, the anode quickly degraded due to carbon deposition (Fig. 14). Post-run XRD

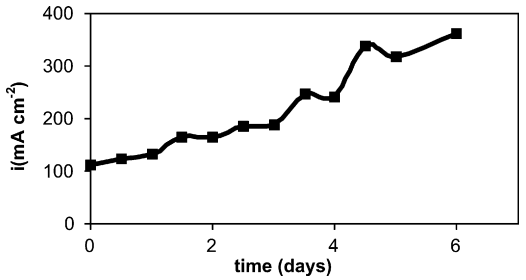

Fig. 13. Current densities measure over a 6-day period in 10% (v/v) H_2S/CH_4 on Co-YSZ at 0.5 V and 850 °C.

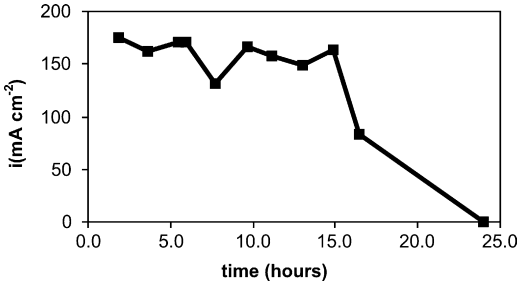

Fig. 14. Current densities measured over a 2-day period in CH_4 on CoS-YSZ at 850 °C.

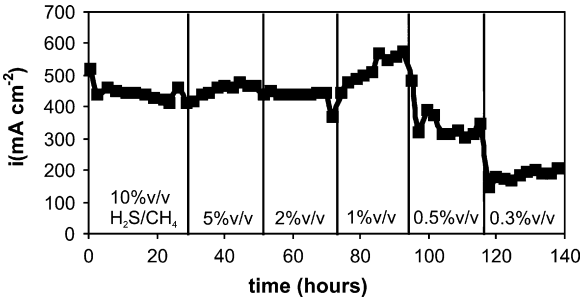

Fig. 15. Current density as a function of time at 850 °C at 0.5 V with changing H_2S content.

analysis showed this anode consisted of Co (PDF# 15-0806), YSZ (PDF# 30-1468) and graphite (PDF# 26-1077). The CoS-species maintained in the fuel cell when H_2S was present was quickly reduced back to elemental Co through sulfidation of CH_4 or H_2 with adsorbed sulfur. Removal of sulfur from the feed, changed the CoS-species to cubic Co and not hexagonal Co, which is the species found when CH_4 was the fuel. Irregardless of crystal structure, carbon formation seems inevitable on Co.

Fig. 15 is a plot of current density at 0.5 V as a function of time for CoS-YSZ in CH_4 with decreasing amounts of H_2S. The anode showed stable performance at each concentration for 24 h and ran for a total of 140 h. Cell performance was stable for concentrations of $H_2S > 1\%$ (v/v). Below 1% (v/v), activity decreased as a function of H_2S partial pressure. The loss in performance may be a result of decreased H_2 production and/or a change in cobalt sulfide stoichiometry to another sulfide species. At low sulfur partial pressures $Co_{1-x}S$ may convert to Co, Co_4S_3 or Co_9S_8 [35].

4. Conclusion

Degradation of the Ni- and Co-based anodes occurred quickly in dry methane. Co-based anodes showed an increase in carbon deposition resistance over Ni-YSZ; however XRD and SEM analysis of the used Co-anodes showed a significant amount of carbon deposition after 15 h.

Metal sulfides, specifically NiS- and CoS-YSZ anodes were active over long periods of time for methane and hydrogen fuels containing H_2S. Electrochemical evaluation of the anode performance via linear voltammetry showed an initial decrease in SOFC performance when H_2S was added to the fuel stream, but after approximately 3 h, when all of the metal was converted to metal-sulfide, the performance recovered and greatly surpassed the initial values. The superior performance suggests metal-sulfides are viable anode materials for carbon, and sulfur resistant SOFC systems. H_2S/H_2 or H_2S/CH_4,CoS-YSZ/YSZ/LSM,air systems systematically exhibited significantly larger exchange current densities over H_2,Co-YSZ/YSZ/LSM,air fuel cells. NiS- also showed a marginal increase in exchange current densities. Mass spectrometry and electrochemical results showed the main fuel was H_2 in H_2S/H_2. Co-based anodes were able to operate in H_2S/CH_4 for up to 6 days without degradation or any visible signs of carbon deposition. The reaction between CH_4 and H_2S resulted in CS_2 production, where any of these gases were possible fuels and could not be distinguished. Carbon deposition quickly ensued when H_2S was removed from the fuel stream and CoS-reduced back to elemental Co.

The addition of H_2S into pure fuel streams enhanced the performance by converting the anodes from pure metal to metal sulfides, suggesting metal-sulfides are appropriate and potentially interesting anode materials for SOFC's with fuels contaminated by sulfur species.

Acknowledgement

The authors thank the Canadian Foundation for Innovation (CFI), the Natural Sciences and Engineering Council of Canada (NSERC) and the University of Ottawa for financial support.

References

[1] J. Liu, S.A. Barnett, Solid State Ionics 158 (2003) 11.
[2] A. Weber, B. Sauer, A.C. Muller, D. Herbstritt, E. Ivers-Tiffee, Solid State Ionics 152–153 (2002) 543.
[3] J.-H. Koh, Y.-S. Yoo, J.-W. Park, H.C. Lim, Solid State Ionics 149 (2002) 157.
[4] R.J. Gorte, S. Park, J.M. Vohs, C. Wang, Adv. Mater. 12 (2000) 1465.
[5] N.C. Triantafyllopoulos, S.G. Neophytides, J. Catal. 217 (2003) 324.
[6] Z. Zhan, Y. Lin, S. Barnett, in: J. Mizusaki (Ed.), Solid Oxide Fuel Cells IX, Electrochemical Society, Quebec City, Quebec, 2005, p. 1321.
[7] Y. Nabae, I. Yamanaka, S. Takenaka, M. Hatano, K. Otsuka, in: J. Mizusaki (Ed.), Solid Oxide Fuel Cells IX, Electrochemical Society, Quebec City, Quebec, 2005, p. 1341.
[8] K. Ahm, S. Lee, J. Vohs, R. Gorte, in: J. Mizusaki (Ed.), Proceedings of the Ninth International Symposium on Solid Oxide Fuel Cells, The Electrochemical Society, Inc., Quebec City, Quebec, 2005, p. 1360.
[9] K. Sasaki, K. Susuki, A. Iyoshi, M. Uchimura, N. Imamura, H. Kusaba, Y. Teraoka, H. Fuchino, K. Tsujimoto, Y. Uchida, N. Jingo, in: S. Singhal, J. Mizusaki (Eds.), International Symposium of Solid Oxide Fuel Cells IX (SOFC-IX), The Electrochemical Society, Inc., Quebec City, Quebec, 2005, p. 1267.
[10] Y. Matsuzaki, I. Yasuda, Solid State Ionics 132 (2000) 261.
[11] S. Xia, V. Birss, in: S. Singhal, J. Mizusaki (Eds.), International Proceedings of Solid Oxide Fuel Cells IX (SOFC-IX), The Electrochemical Society, Inc., Quebec City, Quebec, 2005, p. 1275.
[12] J. Dong, S. Zha, M. Liu, in: S. Singhal, J. Mizusaki (Eds.), International Symposium on Solid Oxide Fuel Cells-IX (SOFC-IX), The Electrochemical Society, Inc., Quebec City, Quebec, 2005, p. 1274.
[13] H. He, R.J. Gorte, J.M. Vohs, Electrochem. Solid State Lett. 8 (2005) A279.
[14] Y.H. Huang, R.I. Dass, Z.-L. Xing, J.B. Goodenough, Science 312 (2006) 254.
[15] R. Mukundan, E.L. Brosha, R.H. Garzon, Electrochem, Solid State Lett. 7 (2004) A5.
[16] C.M. Grgicak, J.B. Giorgi, in: S. Singhal, J. Mizusaki (Eds.), Proceedings of the Ninth International Symposium on Solid Oxide Fuel Cells, The Electrochemical Society, Inc., Quebec City, Quebec, 2005, p. 1200.
[17] C.M. Grgicak, R.G. Green, W.-F. Du, J.B. Giorgi, J. Am. Ceram. Soc. 88 (2005) 3081.
[18] C.M. Grgicak, R.G. Green, J.B. Giorgi, J. Mater. Chem. 16 (2006) 885.
[19] V.V. Krishnan, S. McIntosh, R.J. Gorte, J.M. Vohs, Solid State Ionics 166 (2004) 191.
[20] J. Winkler, P. Hendriksen, N. Bonanos, M. Mogensen, J. Electrochem. Soc. 145 (1998) 1184.
[21] S. Chan, X. Chen, K. Khor, J. Appl. Electrochem. 31 (2001) 1163.
[22] C. Grgicak, J.B. Giorgi, J. Phys. Chem. C 111 (2007) 15446.

[23] S. Jiang, J. Love, L. Apateanu, Solid State Ionics 160 (2003) 15.
[24] M. Guillodo, P. Vernoux, J. Fouleier, Solid State Ionics 127 (2000) 99.
[25] M. Brown, S. Primdahl, M. Mogensen, J. Electrochem. Soc. 2 (2000) 475.
[26] J. Butler, Trans. Faraday Soc. 19 (1923) 729.
[27] J. Butler, Trans. Faraday Soc. 28 (1932) 379.
[28] T. Erdey-Gruz, M. Volmer, Z. Phys. Chem. A 150 (1930) 203.
[29] T. Erdey-Gruz, H. Wick, Z. Phys. Chem. A 162 (1932) 53.
[30] C. Keep, R. Baker, J. France, J. Catal. 47 (1977) 232.
[31] R. Baker, P. Harris, S. Terry, Nature 253 (1975) 37.
[32] R. Baker, P. Harris, J. Henderson, R. Thomas, Carbon 13 (1975) 17.
[33] R. Baker, M. Barber, P. Harris, F. Feates, R. Waite, J. Catal. 1972 (1972) 51.
[34] D. Nava, I. Gonzalez, Electrochem. Acta 51 (2006) 5295.
[35] S. Mrowec, M. Danielewski, A. Wojtowicz, J. Mater. Sci. 33 (1998) 2617.
[36] H. Seim, H. Fjellvag, F. Gronvold, S. Stolen, J. Solid State Chem. 121 (1996) 400.
[37] N.U. Pujare, K.W. Semkow, a.F. Sammells, J. Electrochem. Soc. 134 (1987) 2639.
[38] M. Liu, G. Wei, J. Luo, A.R. Sanger, K.T. Chuang, J. Electrochem. Soc. 150 (2003) A1025.
[39] G. Wei, J. Luo, A. Sanger, K. Chuang, J. New Mater. Electochem. Syst. 8 (2005) 59.
[40] D.R. Peterson, J. Winnick, J. Electrochem. Soc. 145 (1998) 1449.
[41] B.J. Lindberg, K. Hamrin, G. Johansson, U. Gelius, A. Fahlmann, C. Nordling, K. Siegbahn, Phys. Scr. 1 (1970) 286.
[42] J.F Moulder, W.F. Stickle, P.E. Sobol, K.D. Bomben, Handbook of X-ray Photoelectron Spectroscopy, Physical Electronics, Inc., 1995.
[43] R. Fantoni, M. Giorgi, A.G.G. Moliterni, W.C.M. Berden, V. Lazic, O. Martini, F.P. Mattiot, J. Mater. Res. 7 (1992) 1204.
[44] Z. Feng, K. Komvopoulos, J. Appl. Phys. 78 (1995) 2720.
[45] S. Gupta, B.R. Weiner, G. Morell, J. Mater. Res. 18 (2003) 363.
[46] F. Raulin, G. Toupance, Orig. Life 6 (1975) 91.